博士論文

Comprehensive three-dimensional analysis visualizes renal

sympathetic denervation after ischemia/reperfusion injury

（臓器透明化を用いた全腎臓 3 次元解析による

腎交感神経障害の可視化）

長谷川 頌

Comprehensive three-dimensional analysis visualizes renal

sympathetic denervation after ischemia/reperfusion injury

（臓器透明化を用いた全腎臓 3 次元解析による

腎交感神経障害の可視化）

所属：東京大学大学院医学系研究科内科学専攻（腎臓内科学）

指導教員：南学 正臣

氏名：長谷川 頌

Contents

1

Abbreviation lists

3D	three-dimensional
CUBIC	Clear, Unobstructed Brain/Body Imaging Cocktails and Computational analysis
IRI	ischemia-reperfusion injury
RI	refractive index
LSFM	light-sheet fluorescent microscopy
PBS	phosphate buffered saline
PFA	paraformaldehyde
PBST	0.5% (v/v) triton X-100 in PBS
TH	tyrosine hydroxylase
αSMA	alpha smooth muscle actin
AQP2	aquaporin 2
SGLT2	sodium glucose cotransporter 2
FIJI	Fiji is just ImageJ
PACT	Passive CLARITY
NE	norepinephrine
AKI	acute kidney injury
CKD	chronic kidney disease

Abstract

The sympathetic nervous system is critical in maintaining the homeostasis of renal functions. Its three-dimensional (3D) structures in the kidney, however, have not been elucidated because of the limitation of conventional imaging methods. CUBIC (Clear, Unobstructed Brain/Body Imaging Cocktails and Computational analysis) is a newly developed tissue clearing technique, which enables whole-organ 3D imaging without thin-sectioning. Comprehensive 3D imaging by CUBIC has revealed that sympathetic nerves are primarily distributed around arteries in the mouse kidney. Notably, sympathetic innervation density decreased 10 days after ischemia-reperfusion injury (IRI) [voluminal ratio of innervation area to kidney; $5.95 \pm 0.88\%$ (sham; n = 4) vs. $1.76 \pm 0.48\%$ (IRI; n = 4), P = 0.0002]. Moreover, norepinephrine levels in kidney tissue (output of sympathetic nerves) were significantly reduced in injured kidneys [0.39 ± 0.03 ng/mg tissue (healthy; n = 9) vs. 0.09 ± 0.03 ng/mg tissue (injured; n = 9), P < 0.0001], which confirmed the sympathetic denervation after IRI. Time-course imaging data demonstrated that the denervation was persistent even 28 days after IRI, although the innervation partially recovered with time course, indicating sympathetic nervous abnormality during the progression of chronic kidney disease. This new 3D imaging analysis (CUBIC-kidney) can also visualize collecting ducts, proximal tubules

and glomeruli in kidney tissue, providing comprehensive, macroscopic perspective for

kidney research as a strong imaging tool.

Introduction

The sympathetic nervous system plays an important role in maintaining the homeostasis of multiple renal functions. Its three-dimensional (3D) structures in the kidney, however, have not been elucidated because of limitations in conventional imaging methods. Tissue clearing-based 3D imaging is the most promising strategy for the visualization of whole organs without thin-sectioning [1]. There are some tissue-clearing methods of whole organs according to the developers of each protocol; CUBIC (Clear, Unobstructed Brain/Body Imaging Cocktails and Computational analysis) [2-6], AbSca*l*e (Sca*l*eS) [7, 8], iDISCO [9, 10], and CLARITY [11, 12]. Among these protocols, CUBIC has been improved to make a whole organ or body highly transparent by using an efficient delipidation cocktail and an optimized refractive index (RI)-matching medium, which are compatible with 3D immunohistochemistry [5, 6]. The combination of tissue clearing, 3D immunohistochemistry, and light-sheet fluorescent microscopy (LSFM) enables high-throughput imaging of whole tissue. Here, I established the whole-kidney 3D analysis using the CUBIC protocol and visualized the 3D structure of renal sympathetic nerves, revealing their abnormalities after ischemia-reperfusion injury (IRI).

Materials and Methods

Preparation of tissue clearing solutions (CUBIC)

CUBIC-L for decolorization and delipidation was prepared as a mixture of 10 w% polyethylene glycol mono-p-isooctylphenyl ether/Triton X-100 (12967-45, Nacalai Tesque, Kyoto, Japan) and 10 w% N-buthyldiethanolamine (B0725, Tokyo Chemical Industry, Tokyo, Japan). CUBIC-R was prepared as a mixture of 45 w% 2,3-dimethyl-1-phenyl-5-pyrazolone/antipyrine (D1876, Tokyo Chemical Industry) and 30 w% nicotinamide (N0078, Tokyo Chemical Industry). CUBIC-R+ for RI matching was prepared by adding 0.5 v% N-buthyldiethanolamine to CUBIC-R.

Animal experiments of ischemia-reperfusion injury (IRI)

C57BL/6 mice were obtained from CLEA Japan, Inc. (Tokyo, Japan). All animal procedures were performed according to the National Institutes of Health guidelines (Guide for the Care and Use of the Laboratory Animals). All experiments were approved by the Tokai University Institutional Review Board and performed under the guidelines of the Tokai University Committee (Approval numbers: 171086 and 182043). Male mice were anesthetized by the inhalation of isoflurane and intraperitoneal administration of pentobarbital sodium (50 mg/kg). Renal IRI was

performed by clamping the renal pedicles for 45 minutes. The clamps were removed, and the wound was sutured after restoration of blood flow was visually observed. Sham-operated mice underwent the same procedure, without clamping of renal pedicles. Body temperature was maintained by placement of the mice on a 28°C heating table during the procedure.

Animal experiments of alloxan-induced diabetic mice

Crl:CD1 (ICR) mice were obtained from Charles River Laboratories Japan Inc. (Japan). All experiments were approved by the University of Tokyo Institutional Review Board (approval number: P17-110). Animals were divided into three groups: Control (normal animals eating normal food), Diabetes (diabetic animals eating normal food) and Diabetes + enarodustat (diabetic animals eating food mixed with the oral hypoxia-inducible factor stabilizer enarodustat). Alloxan administration (90 mg/kg) was utilized for inducing diabetes. Vehicle (for Control) or 90 mg/kg of alloxan (for Diabetes) were intravenously administered into mice 3 days before grouping. Kidney samples were obtained 16 days after grouping.

Kidney sampling and CUBIC protocol for tissue clearing

The mice were euthanized by an overdose of pentobarbital sodium (> 100 mg/kg) and perfused with 20 ml of phosphate buffered saline (PBS) (pH 7.4) and 30 ml of 4% paraformaldehyde (PFA) in phosphate buffer (09154-85, Nacalai Tesque) through the left ventricle of the heart. The kidneys were fixed in 4% PFA at 4°C for 16 hours, then washed with PBS for 2 hours, three times before the clearing process. The fixed kidneys were immersed in 50% (v/v) CUBIC-L (1:1 mixture of water and CUBIC-L) for 6 hours and then immersed in CUBIC-L with shaking at 37°C for 5 days. CUBIC-L was daily refreshed during this process. After the delipidation process, kidneys were washed with PBS at room temperature for 2 hours, three times; they were immersed in 50% (v/v) CUBIC-R+ (1:1 mixture of water and CUBIC-R+) for 1 day, and then in CUBIC-R+ with gentle shaking for 2 days. These samples were sufficiently transparent to acquire inner fluorescent data (Figure 1A, B).
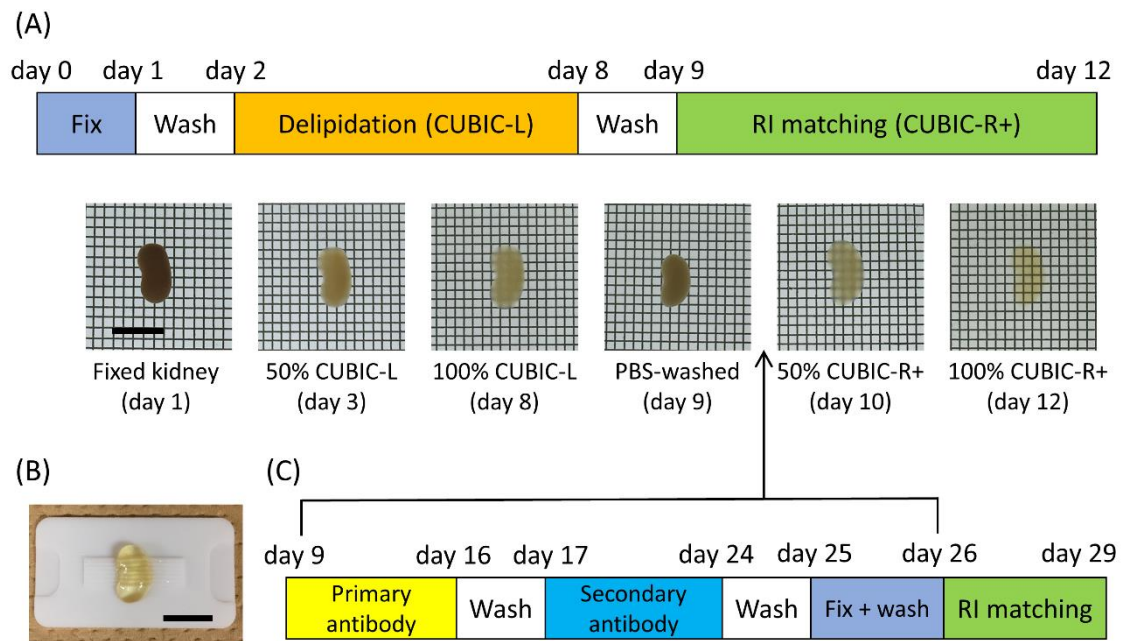
Figure 1. Tissue clearing and immunofluorescent staining of kidneys by CUBIC

(A) Tissue clearing protocol and bright-field images are shown for each step. Scale bar: 10 mm. (B) Optically cleared kidney, observed by light-sheet fluorescent microscopy (LSFM). Scale bar: 10 mm. (C) Three-dimensional immunofluorescent staining protocol with primary and secondary antibodies. Kidney samples are subjected to immunofluorescent staining after delipidation, followed by refractive index (RI) matching.

3D immunofluorescent staining

Delipidated kidneys were immunostained with primary antibodies in the staining buffer composed of 0.5% (v/v) Triton X-100, 0.5% casein (37528, Thermo Fisher Scientific, Waltham, MA, USA) and 0.05% sodium azide (195-11092, Wako, Osaka, Japan) for 7 days at 37°C with shaking (Figure 1C). The samples were washed with 0.5% (v/v) triton X-100 in PBS (PBST) for 1 day, then immunostained with secondary antibodies in the staining buffer composed of 0.5% (v/v) Triton X-100, 0.1% casein and 0.05% sodium azide for 7 days at 37°C with shaking. The samples were washed with PBST for 1 day, post-fixed by 1% formaldehyde (16223-55 Nacalai Tesque) in phosphate buffer for 3 hours, washed with PBS for at least 6 hours, and then immersed in 50% CUBIC-R+.

Primary antibodies used for staining were anti-tyrosine hydroxylase (TH) antibody (sheep polyclonal, 1:100, ab113, Abcam, Cambridge, UK), anti-alpha smooth muscle actin (αSMA) antibody (rabbit polyclonal, 1:200, ab5694, Abcam), anti-aquaporin 2 (AQP2) antibody (rabbit monoclonal, 1:100, ab199975, Abcam), anti-sodium glucose cotransporter 2 (SGLT2) antibody (rabbit polyclonal, 1:100, ab85626, Abcam) and anti-podocin antibody (rabbit polyclonal, 1:100, P0372, Sigma-Aldrich, St. Louis, USA). Secondary antibodies used for staining were Alexa Flour 555-conjugated

donkey anti-sheep IgG (1:100, A-21436, Invitrogen, Carlsbad, USA) and Alexa Flour

647-conjugated donkey anti-rabbit IgG (1:200, A-31573, Invitrogen).

Lectin perfusion of kidneys

The mouse was anesthetized by the inhalation of isoflurane, followed by the

perfusion with 5 mg/kg of DyLight 649 Lycopersicon Esculentum (Tomato) Lectin

(DL-1178, VECTOR LABORATORIES, INC., Burlingame, USA) from the left

ventricle of the heart. Five minutes later, the mouse was perfused with 20 ml of PBS

(pH 7.4) and 30 ml of 4% PFA in phosphate buffer. After kidney sampling, the process

of fixation and tissue-clearing was the same as other kidneys. The lectin-perfused

kidney was immunostained with anti-αSMA-Cy3 conjugated antibody (mouse

monoclonal, 1:100, C6198, Sigma-Aldrich).

Image acquisition, 3D reconstruction and quantification analysis

Comprehensive 3D kidney images were acquired with a custom-built LSFM

(MVX10-LS, developed by Olympus, Tokyo, Japan) (Figure 2) [5, 6]. Images were

captured by using a 0.63× objective lens (numerical aperture = 0.15, working distance =

87 mm), with 1.6× optical zoom. The pixel size of each obtained image was x = 6.45

μm and y = 6.45 μm; z-step was set to 7 μm. Lasers of 532 nm and 639 nm were used

for image acquisition. The RI-matched kidney was immersed in a 55:45 mixture of

silicon oil HIVAC-F4 (RI = 1.555, Shin-Etsu Chemical Co., Ltd., Tokyo, Japan) and

mineral oil (RI = 1.467, M8410, Sigma-Aldrich) during image acquisition (RI = 1.51).

All raw image data were collected in a 16-bit TIFF format. 3D-rendered images were

visualized and captured with Imaris software (Bitplane, Belfast, UK). Quantifications of

the voluminal ratio of signal positive area (TH and αSMA) to kidney were performed by
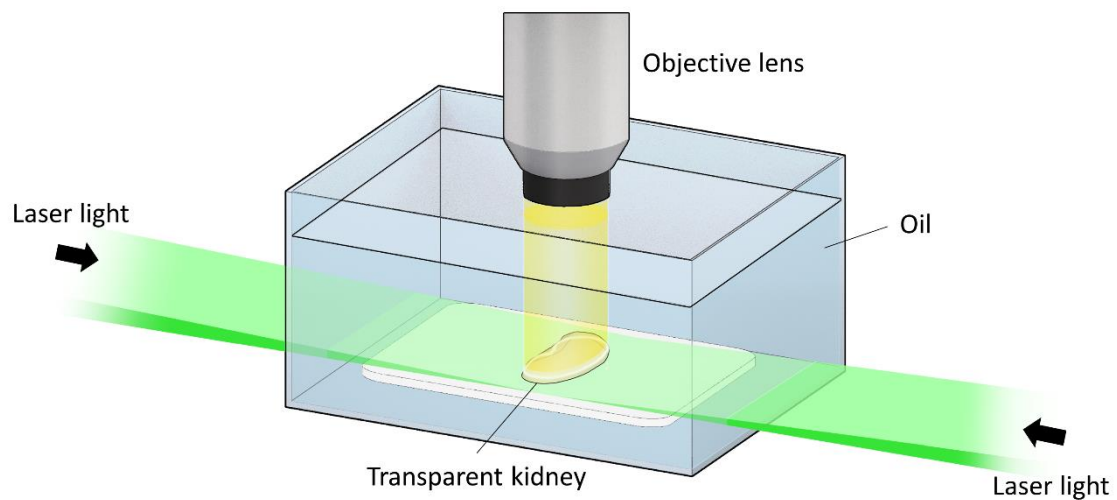
FIJI (Fiji is just ImageJ) software.

Figure 2. Comprehensive three-dimensional (3D) imaging by light-sheet fluorescent
microscopy (LSFM)
The transparent kidney is immersed in oil (RI = 1.51) during image acquisition. A light
sheet is illuminated from both sides of the sample and excitation signals are acquired
from its vertical side through the objective lens. The stage moves in the axial direction
and z-stack images are quickly obtained. When the stage moves in the axial direction,
the objective lens synchronically moves in the axial direction to avoid defocusing. The
characteristics of LSFM enable high-throughput z-stack imaging of transparent samples.

Other tissue-clearing protocols

Sca*l*eS: SCALEVIEW-S Trial Kit (299-79901, Wako) was utilized. The kidney

fixed with 4% PFA was incubated in SCALEVIEW-S0 for 12 hours at 37℃, in

SCALEVIEW-S1 for 12 hours at 37℃, in SCALEVIEW-S2 for 12 hours at 37℃, and

in SCALEVIEW-S3 for 12 hours at 37℃. The sample was then washed with PBS for 12

hours at 4℃ and incubated in SCALEVIEW-S4 for 12 hours at 37℃. Finally, the

sample was incubated in SCALEVIEW-SMt for 12 hours at room temperature.

iDISCO: The kidney fixed with 4% PFA was incubated overnight in 10 ml of

50% v/v tetrahydrofuran/H_2O (186562, Sigma-Aldrich). The sample was then incubated

for 1 hour in 10 ml of 80% tetrahydrofuran/H_2O, twice 1 hour in 100% tetrahydrofuran

and 1 hour in dichloromethane (270997, Sigma-Aldrich). Finally, the sample was

incubated in 15 ml of dibenzyl ether (108014, Sigma-Aldrich) for 1 day. All procedures

were conducted at room temperature. Organic solvents were handled in the fume hood.

Passive CLARITY (PACT): "Hydrogel solution" was prepared by mixing 40

ml of 40% (w/v) acrylamide (011-08015, Wako), 10 ml of 2% (w/v) bis-acrylamide

(138-0632, Wako), 40 ml of 10 × PBS (163-25265, Wako), 100 ml of 16% PFA (553-

87281, Wako), 1 g of VA-044 (223-02112, Wako) and 210 ml of distilled water.

"Clearing solution" was prepared by mixing 20 g of Sodium dodecyl sulfate, 6.183 g of

boric acid (021-02195, Wako) into distilled water, making up to 500 ml after adjusting

pH to 8.5 with NaOH. "Boric acid buffer" was prepared by mixing 0.2 M boric acid

(adjusted pH to 8.5) with 0.1% (v/v) Triton X-100 (12967-45, Nacalai Tesque). The

kidney fixed with 4% PFA was incubated in hydrogel solution at 4℃ for 2 days, which

was transferred to 37℃ water baths and gently shaken for 4 hours until the hydrogel

fully solidified. The sample was extracted from the solidified hydrogel and washed with

clearing solution with 2 changes for 1 day. The sample was then immersed in clearing

solution (daily refreshed) with gentle shaking at 37℃ for 8 days. After being washed

with boric acid buffer (daily refreshed) at 37℃ for 3 days, the sample was immersed in

87% (v/v) glycerol (079-00614, Wako) at room temperature for 3 days.

Quantification of norepinephrine (NE) levels in kidney tissue

The mice were euthanized by cervical dislocation and kidneys were quickly

removed and put into liquid nitrogen. The frozen kidneys were homogenized in 900 μl

of 0.2 M perchloric acid containing 100 μM EDTA 2Na and 100 ng of 3,4-

dihydroxybenzylamine hydrobromide as an internal standard and kept at 4℃ for 30

minutes. Homogenates were centrifuged at 20,000 × g for 15 minutes at 4℃. The

supernatants were collected, adjusted to pH 3.0 with 1.0 M CH_3COONa and analyzed

by the high-performance liquid chromatography system with an electrochemical

detector (HTEC-500, Eicom, Kyoto, Japan).

Statistical analysis

All the data were expressed as mean ± SD. Comparisons were performed by

unpaired t-tests. All statistical analyses were performed with JMP® Pro 14.0.0 (SAS

Institute Inc., Cary, NC, USA).

Results

CUBIC and other tissue-clearing methods

Four tissue clearing protocols (CUBIC, Sca*l*eS, iDISCO and PACT) were
compared from the viewpoint of compatibility with whole-kidney samples. Since the
CUBIC protocol accomplished a high degree of transparency compared with other
protocols (Figure 3), I applied this protocol to my study.

Figure 3. CUBIC and other tissue-clearing protocols
Kidneys were subjected to four tissue-clearing methods: CUBIC, Sca*l*eS, iDISCO and
Passive CLARITY (PACT). CUBIC has accomplished a high degree of transparency,
which is compatible with the observation by a light-sheet fluorescent microscopy,
compared with other tissue-clearing protocols. Scale bar: 10 mm.

Tissue clearing and 3D imaging of renal arteries and sympathetic nerves

Kidneys isolated from adult male mice were optically cleared using CUBIC

protocol (Figure 1A, 1B), then were cut in half and subjected to immunofluorescent

staining with anti-TH antibody and anti-αSMA antibody between delipidation and RI-

matching processes (Figure 1C). These samples were sufficiently transparent to acquire

inner fluorescent data by LSFM, which uses separate excitation-detection paths (Figure

2). The characteristics of LSFM are beneficial for rapidly acquiring z-stack images [1,

13] and accomplishing high-throughput analysis of transparent kidneys labeled with

fluorescent antibodies. From each kidney sample, 400 to 600 z-stack images (z = 7 μm,

pixel size; x = 6.45 μm, y = 6.45 μm) were obtained (Figure 4). 3D reconstructions of z-

stack (x-y plane) images successfully visualized the 3D structures of sympathetic nerves

(TH) and arteries (αSMA) in the kidney (Figure 5). The merged image has illustrated

that sympathetic nerves travel around arteries, suggesting that the function of renal

arteries is controlled by sympathetic nerves (Figure 5). I also conducted the

conventional two-dimensional immunofluorescent staining of a thin-sliced section,

confirming that sympathetic nerves are distributed around arteries, although the 3D

structures could not be grasped (Figure 6). In this manner, 3D imaging by CUBIC

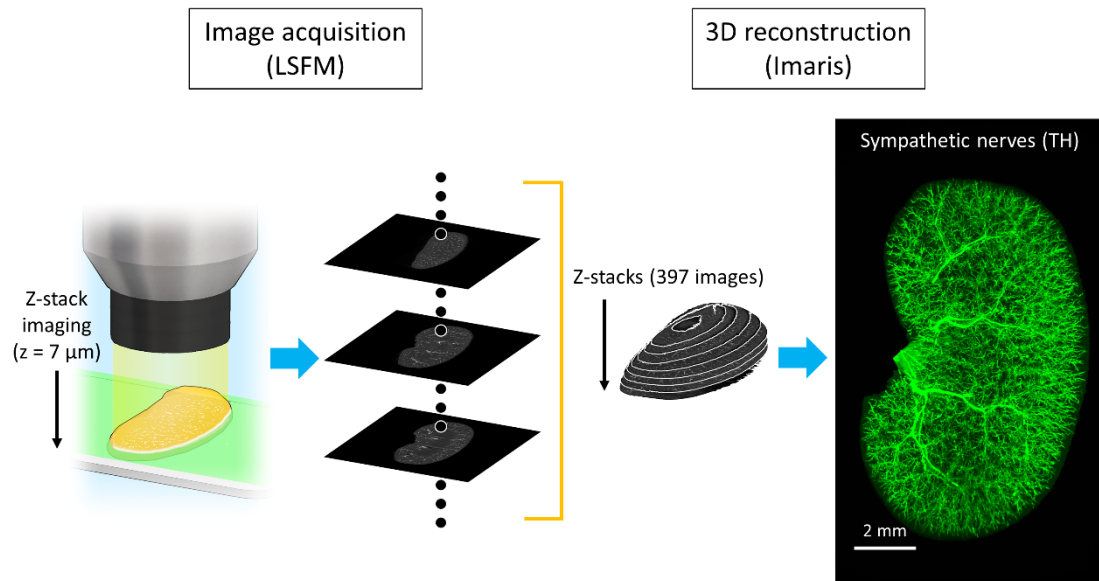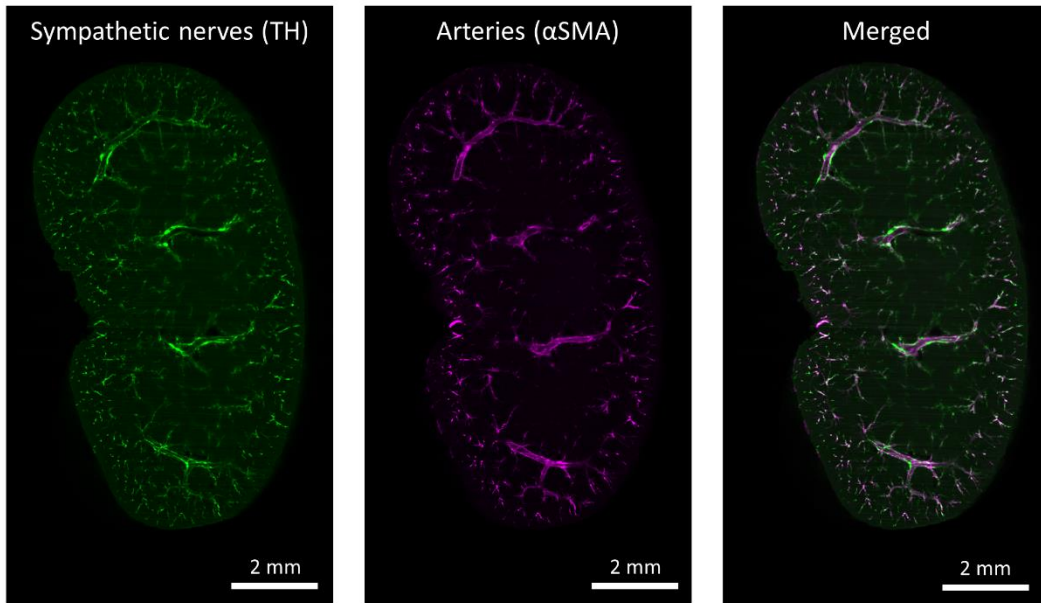provided comprehensive, macroscopic understanding of kidney anatomy.

Figure 4. Image acquisition and three-dimensional (3D) reconstruction of z-stack images

Z-stack images of transparent kidney are acquired by light-sheet fluorescent microscopy (LSFM). The kidney is subjected to immunofluorescent staining with anti-tyrosine hydroxylase (TH) antibody and anti-α-smooth muscle actin (αSMA) antibody. Each signal can be obtained by using the laser and filter corresponding to each fluorescent antibody. The z-stack images are 3D-reconstructed by Imaris software (Bitplane, Switzerland). The right panel is the 3D-reconstructed (volume rendering) image of TH expression (normal kidney).

(A) x-y plane images (z = 1.78 mm)

Sympathetic nerves (TH) | Arteries (αSMA) | Merged

(B) 3D-reconstructed images

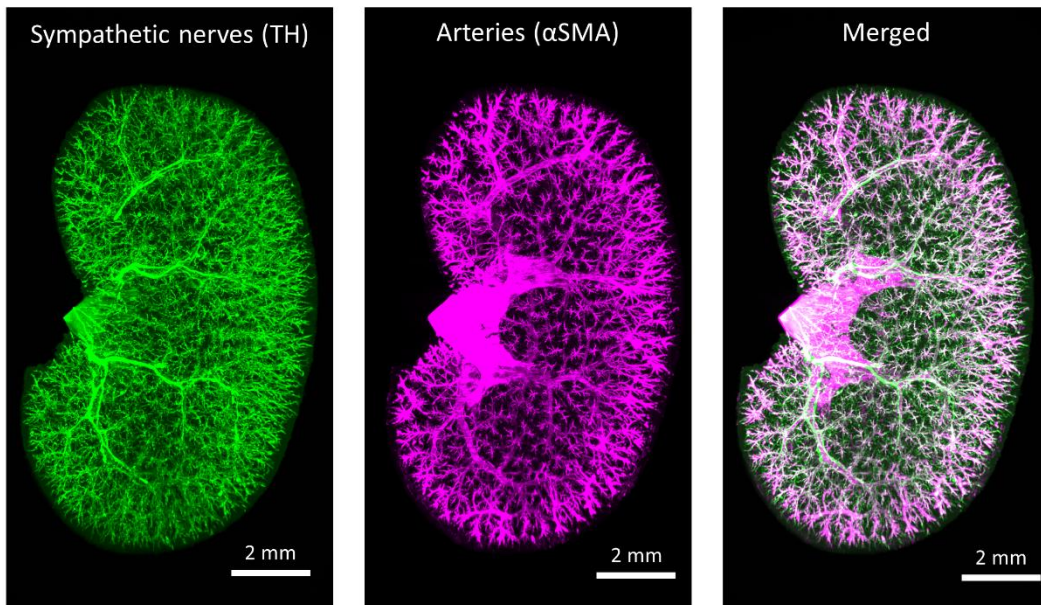Sympathetic nerves (TH) | Arteries (αSMA) | Merged

<u>Figure 5. Three-dimensional (3D) distribution of sympathetic nerves and arteries in the kidney</u>

The kidney was subjected to immunofluorescent staining with anti-tyrosine hydroxylase (TH) antibody and anti-alpha smooth muscle actin (αSMA) antibody. (A) x-y plane images and (B) 3D-reconstructed images are shown. 3D images were reconstructed from 397 z-stack (x-y plane) images. Sympathetic nerves (TH, green) were primarily distributed in parallel with arteries (αSMA, magenta). This kidney was used in Figure 4.
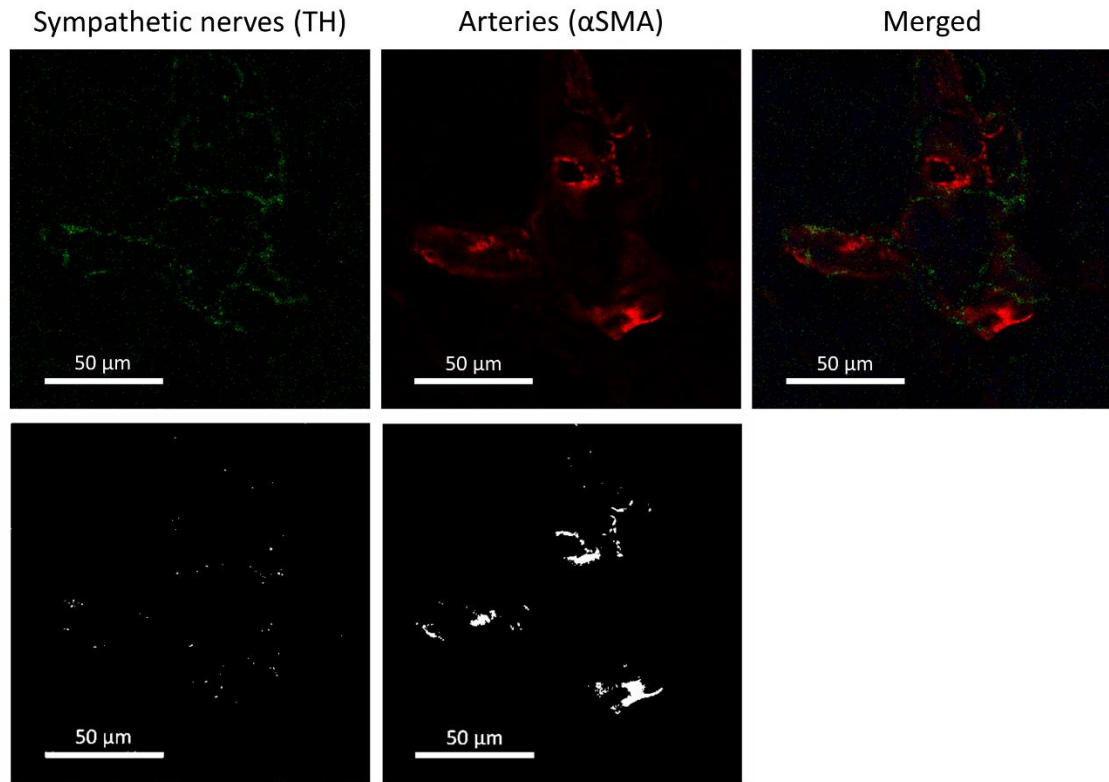
Figure 6. Conventional two-dimensional immunofluorescent staining of a thin-sliced section

The thin-sliced section of a frozen kidney was subjected to immunofluorescent staining with anti-tyrosine hydroxylase (TH) antibody and anti-alpha smooth muscle actin (αSMA) antibody, showing that sympathetic nerves are primarily distributed around arteries, although the three-dimensional structures cannot be grasped. Lower pictures are binary converted version of upper pictures. Scale bar: 50 μm.

Quantification of the ratio of signal positive volume in transparent kidney

A method to quantify 3D immunofluorescent information of kidney tissue was

used to compare imaging data obtained by LSFM. In brief, I performed binary

conversion and calculated the integral of the area of interest (Figure 7 shows an example

of this method). The analyses were rapidly and automatically performed by macro-

execution in Fiji (a distribution of ImageJ) [14]. The ratio of signal (TH or αSMA)

positive volume to the kidney was adopted to enable quantitative comparison between
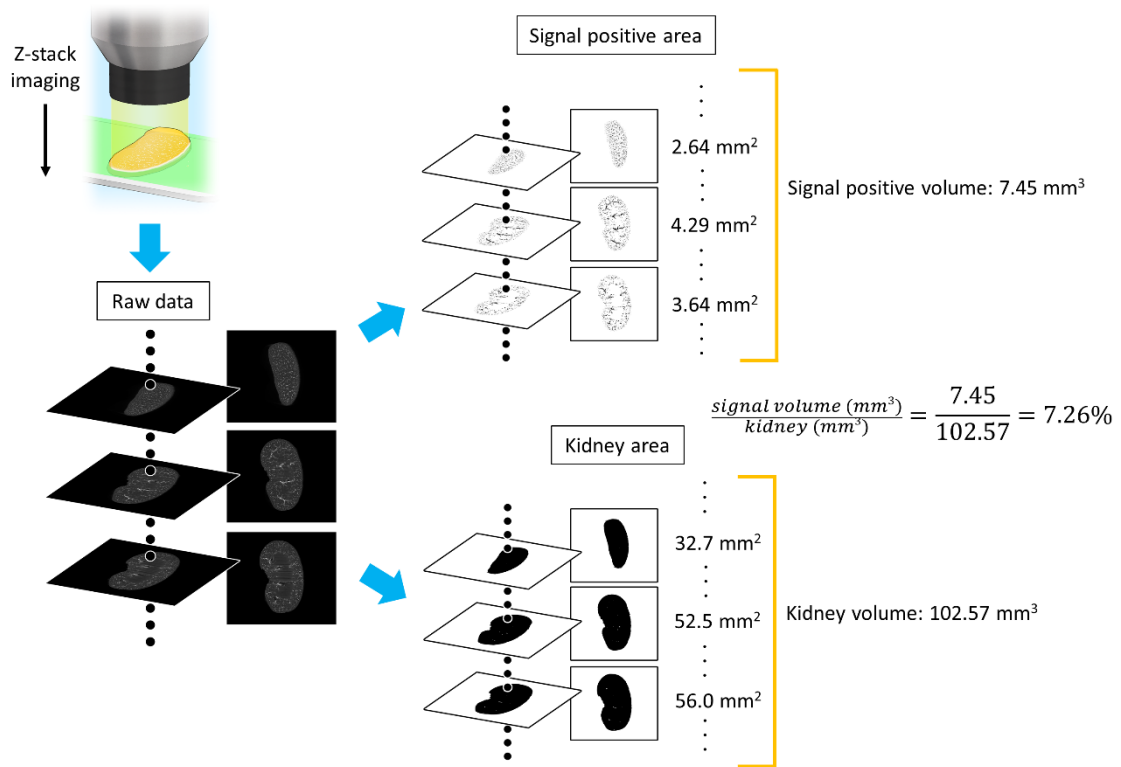
different samples.

Figure 7. Quantification of the ratio of signal positive volume to the kidney
The process of calculating the ratio of signal (TH)-positive volume to total kidney
volume is shown. This kidney was used in Figure 4 and 5. The appropriate thresholds
for covering signal-positive areas or covering total kidney areas are set by using Fiji
software. The raw data are binary converted, according to each threshold. The signal-
positive area and total kidney area of each z-stack are automatically calculated by
macro-execution. The volumes of interest can be obtained by calculating the integral
(each voxel size: x = 6.45 μm, y = 6.45 μm, z = 7 μm).

Visualization of abnormal sympathetic nerves after renal IRI

Renal IRI is caused by sudden occlusion of renal blood flow and is often used as an acute kidney injury (AKI) model. Because it is well known that IRI causes gradual renal fibrosis after acute inflammation, analyzing morphological or functional changes in the kidney after IRI can present important information regarding the mechanism of AKI to chronic kidney disease (CKD) progression. Therefore, I evaluated immunofluorescent changes between normal and injured kidneys.

Eight-week-old male C57BL/6 mice underwent sham operation or bilateral IRI for 45 minutes, then were euthanized 10 days after surgery. The kidneys were optically cleared by using the CUBIC protocol, then stained for TH and αSMA expression by 3D immunofluorescent staining, and observed by LSFM. 3D imaging data clearly visualized reduced sympathetic innervation 10 days after IRI (Figure 8 and 9). The ratio of TH positive volume to the kidney was significantly reduced in IRI-operated mice, compared with sham-operated mice [$5.95 \pm 0.88\%$ (sham; n = 4) vs. $1.76 \pm 0.48\%$ (IRI; n = 4), P = 0.0002] (Figure 10A), suggesting functional abnormality of sympathetic nerves after IRI. In contrast, the ratio of αSMA-positive volume to total kidney volume does not significantly differ at this stage [$4.62 \pm 1.21\%$ (sham; n = 4) vs. $5.00 \pm 1.03\%$ (IRI; n = 4), P = 0.65] (Figure 10B).

TH　　　　　　αSMA　　　　　　Merged

Sham (day 10)

$$\frac{TH\ volume\ (mm^3)}{kidney\ (mm^3)} = \frac{8.15}{164.46} = 4.96\%$$

$$\frac{\alpha SMA\ volume\ (mm^3)}{kidney\ (mm^3)} = \frac{6.52}{164.46} = 3.97\%$$

IRI (day 10)

$$\frac{TH\ volume\ (mm^3)}{kidney\ (mm^3)} = \frac{2.75}{131.63} = 2.09\%$$

$$\frac{\alpha SMA\ volume\ (mm^3)}{kidney\ (mm^3)} = \frac{6.48}{131.63} = 4.92\%$$
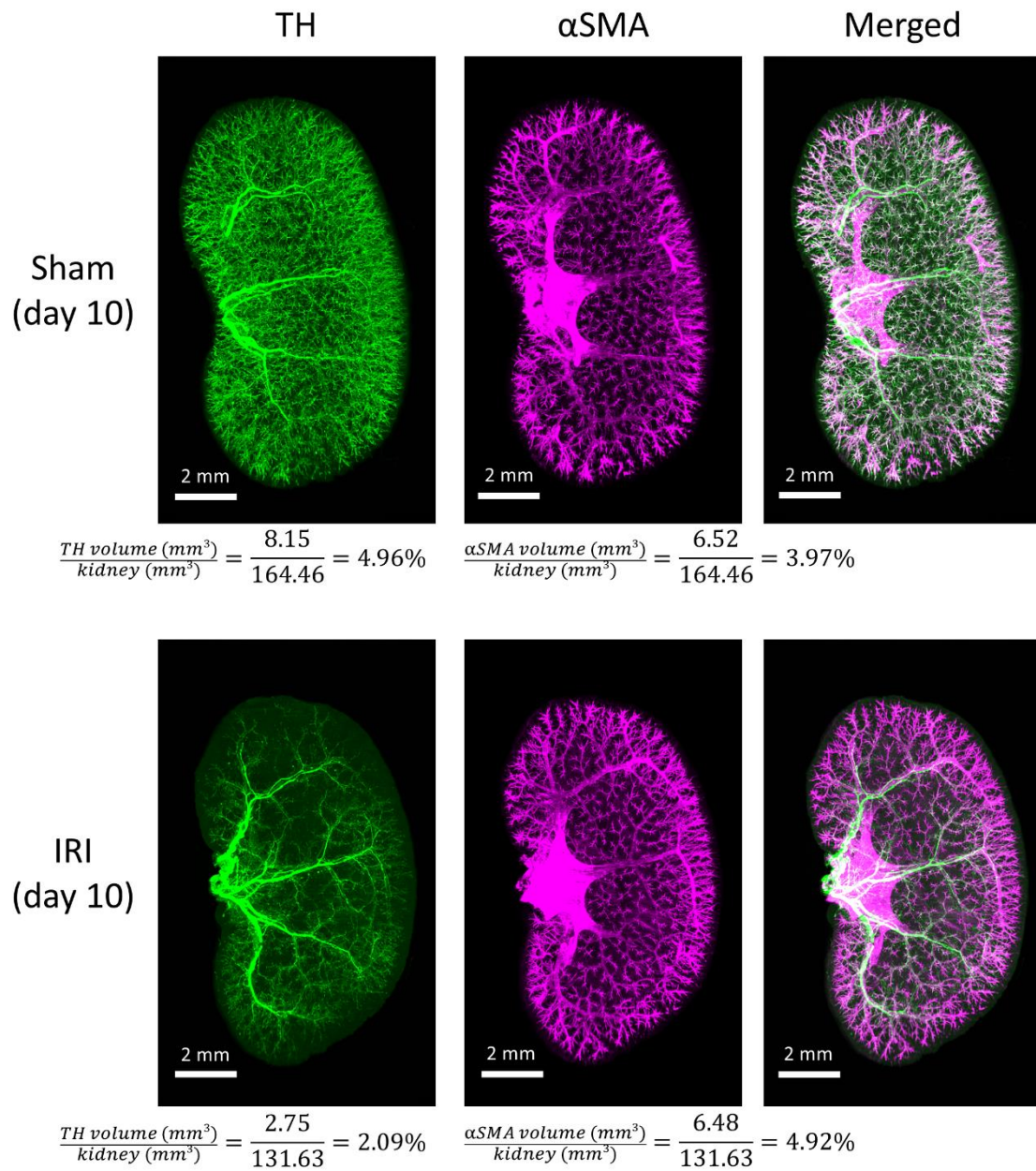
Figure 8. Abnormal sympathetic nerves 10 days after ischemia-reperfusion injury (IRI) Comparison of three-dimensional (3D) images between sham (upper) and IRI (lower). TH; tyrosine hydroxylase (green), αSMA; alpha-smooth muscle actin (magenta). The volumes of interest (TH-positive, αSMA-positive, and whole kidney) were calculated as shown in Figure 7. 3D images and quantification analysis of other kidneys are presented in Figure 9.

(A) Sham

TH αSMA Merged

$$\frac{TH\ volume\ (mm^3)}{kidney\ (mm^3)} = \frac{9.11}{155.16} = 5.87\%$$

$$\frac{\alpha SMA\ volume\ (mm^3)}{kidney\ (mm^3)} = \frac{6.35}{155.16} = 4.09\%$$

$$\frac{TH\ volume\ (mm^3)}{kidney\ (mm^3)} = \frac{7.57}{106.72} = 7.09\%$$

$$\frac{\alpha SMA\ volume\ (mm^3)}{kidney\ (mm^3)} = \frac{6.87}{106.72} = 6.44\%$$

$$\frac{TH\ volume\ (mm^3)}{kidney\ (mm^3)} = \frac{8.91}{151.97} = 5.86\%$$

$$\frac{\alpha SMA\ volume\ (mm^3)}{kidney\ (mm^3)} = \frac{6.07}{151.97} = 3.99\%$$

(B) IRI

TH αSMA Merged

$$\frac{TH\ volume\ (mm^3)}{kidney\ (mm^3)} = \frac{1.35}{118.10} = 1.14\%$$

$$\frac{\alpha SMA\ volume\ (mm^3)}{kidney\ (mm^3)} = \frac{5.43}{118.10} = 4.60\%$$

$$\frac{TH\ volume\ (mm^3)}{kidney\ (mm^3)} = \frac{1.70}{105.06} = 1.62\%$$

$$\frac{\alpha SMA\ volume\ (mm^3)}{kidney\ (mm^3)} = \frac{6.77}{105.06} = 6.45\%$$

$$\frac{TH\ volume\ (mm^3)}{kidney\ (mm^3)} = \frac{3.18}{145.12} = 2.19\%$$

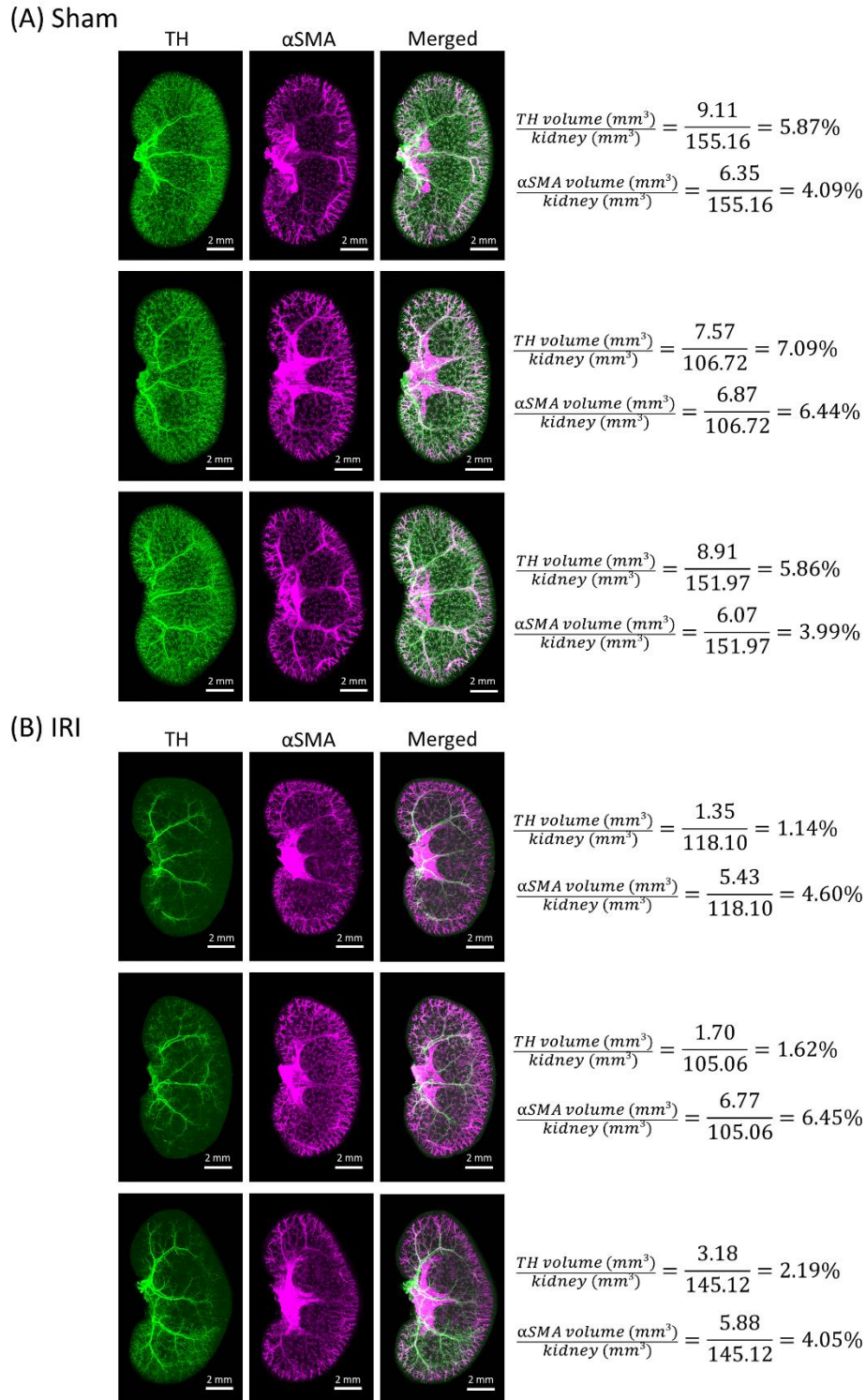$$\frac{\alpha SMA\ volume\ (mm^3)}{kidney\ (mm^3)} = \frac{5.88}{145.12} = 4.05\%$$

Figure 9. Abnormal sympathetic nerves 10 days after ischemia-reperfusion injury (IRI)
Three-dimensional images and quantification analysis of other kidneys are shown. TH; tyrosine hydroxylase (green), αSMA; alpha-smooth muscle actin (magenta). The volumes of interest (TH-positive, αSMA-positive, and whole kidney) were calculated as shown in Figure 7. Scale bar: 2 mm.
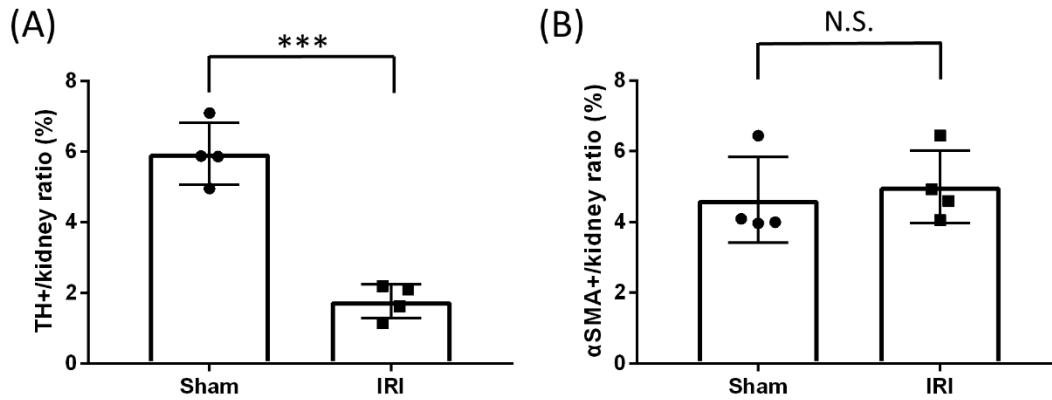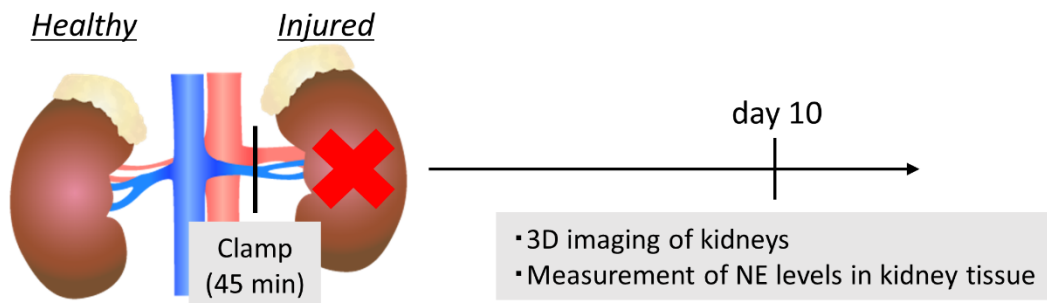
Figure 10. Statistical analysis of signal positive volume 10 days after ischemia-reperfusion injury (IRI)

Statistical analysis of kidneys in Figure 8 and 9 are shown. (A) TH-positive volume/total kidney volume ratio was significantly reduced in IRI, compared with sham (n = 4, ***P = 0.0002). (B) αSMA-positive volume/total kidney volume ratio was not significantly different (n = 4, N.S.; not significant, P = 0.65). All data represent mean ± SD.
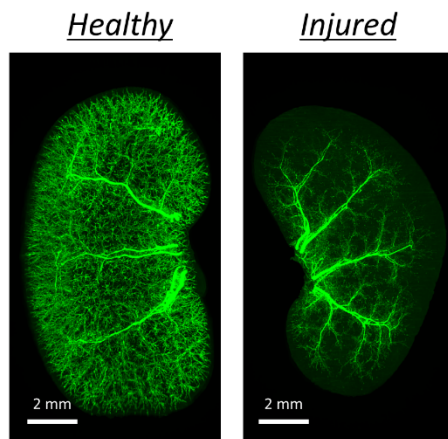
NE levels in kidney tissue after IRI

Although the 3D immunofluorescent data strongly suggest the reduced

sympathetic innervation after IRI, loss of immunoreactivity is not sufficient to signify

sympathetic denervation. Thus, I have confirmed the sympathetic denervation after IRI

in another way, the measurement of NE levels in the kidney tissue (Figure 11A). It is

well known that sympathetic nerves control the function of blood vessels in various

organs by regulating the secretion of NE. In other words, if the denervation really

occurs after IRI, NE levels in the kidney tissue will decrease. In order to remove the

systemic change of NE in blood between mice, I have utilized the unilateral IRI model,

which shows the decreased sympathetic innervation 10 days after IRI (Figure 11B). NE

levels in kidney tissue measured by the high-performance liquid chromatography were

significantly reduced in injured kidneys compared with healthy kidneys [0.39 ± 0.03

ng/mg tissue (healthy; n = 9) vs. 0.09 ± 0.03 ng/mg tissue (injured; n = 9), $P < 0.0001$

(10 days after surgery)], which confirmed the sympathetic denervation after IRI (Figure

11C).

(A) Protocol

Healthy   Injured

Clamp (45 min)

day 10

・3D imaging of kidneys
・Measurement of NE levels in kidney tissue

(B) 3D imaging of kidneys

Healthy   Injured

2 mm   2 mm

(C) NE levels in kidney tissue

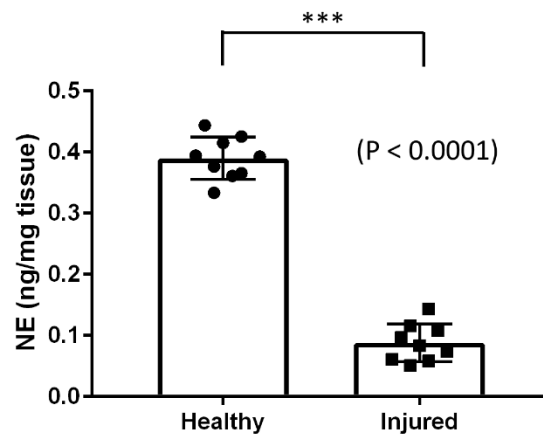*** (P < 0.0001)

NE (ng/mg tissue)

Healthy   Injured

Figure 11. Norepinephrine (NE) levels in kidney tissue were reduced after ischemia-reperfusion injury (IRI)

(A) Eight-week-old mice were subjected to unilateral IRI and euthanized 10 days after surgery. (B) Three-dimensional (3D) imaging by CUBIC revealed that the sympathetic innervation density was reduced in injured kidneys compared with the counterpart healthy kidneys. (C) Norepinephrine (NE) levels in kidney tissue (the output of sympathetic nerves) were significantly reduced in injured kidneys compared with healthy kidneys [0.39 ± 0.03 ng/mg tissue (healthy; n = 9) vs. 0.09 ± 0.03 ng/mg tissue (injured; n = 9), $P < 0.0001$ (10 days after surgery)], which confirmed the sympathetic denervation after IRI. All data represent mean ± SD.

Time-course of sympathetic denervation after IRI

In order to know the time-course of sympathetic denervation, I have conducted

3D imaging of sympathetic nerves in kidneys at different time points (Figure 12). The

sympathetic denervation was persistent even 28 days after IRI, although the innervation

was reduced at day 4 by 86% and partially recovered with time course, indicating

sympathetic nervous abnormality during the progression of CKD [$5.69 \pm 1.33\%$ (sham;

n = 4) vs. $0.78 \pm 0.28\%$ (IRI; n = 4), P = 0.0004 (4 days after surgery), $5.95 \pm 0.88\%$

(sham; n = 4) vs. $1.76 \pm 0.48\%$ (IRI; n = 4), P = 0.0002 (10 days after surgery), $5.67 \pm$

1.00% (sham; n = 4) vs. $3.04 \pm 1.07\%$ (IRI; n = 4), P = 0.01 (28 days after surgery)].
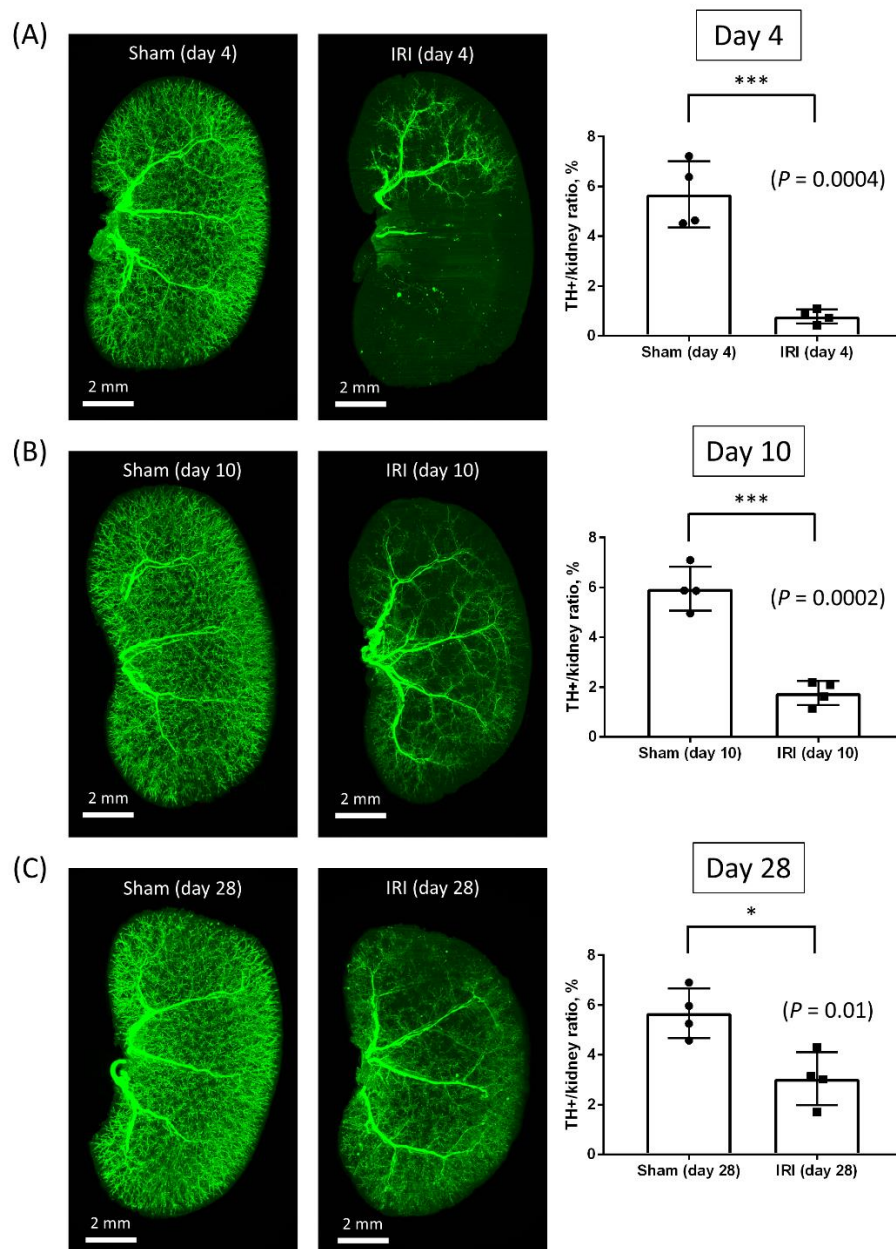
Figure 12. Time-course of sympathetic denervation after ischemia-reperfusion injury (IRI)

Time-course imaging of sympathetic nerves after ischemia-reperfusion injury (IRI); (A) day 4, (B) day 10 (same as Figure 8), (C) day 28. The sympathetic denervation was persistent even 28 days after IRI, although the innervation was drastically reduced at day 4 and partially recovered with time course [5.69 ± 1.33% (sham; n = 4) vs. 0.78 ± 0.28% (IRI; n = 4), P = 0.0004 (4 days after surgery), 5.67 ± 1.00% (sham; n = 4) vs. 3.04 ± 1.07% (IRI; n = 4), P = 0.01 (28 days after surgery)]. All data represent mean ± SD.

29

Other applications of CUBIC-kidney

The CUBIC-based renal 3D imaging analysis (CUBIC-kidney) visualized many other structures in the kidney from comprehensive, macroscopic perspective. I succeeded in visualizing the structure of collecting ducts (AQP2), early segments of proximal tubules (SGLT2) and glomeruli (podocin) (Figure 13A). Moreover, the spatial distribution of glomeruli and arteries was visualized by combining fluorescent labeled-lectin perfusion and 3D immunofluorescent staining with αSMA (Figure 13B). Glomeruli, in which capillaries are highly accumulated, were conspicuously recognized after lectin perfusion in a macroscopic viewpoint, while lectin perfusion labels all the vascular endothelial cells. The 3D imaging of lectin and αSMA showed that glomeruli were botryoidally distributed around arteries in the kidney.

The comprehensive analysis by CUBIC-kidney also clarified the alterations of glomerular volume occurring in the early stages of diabetic kidney disease (Figure 14). Whereas glomerulomegaly was noticeable in the diabetic kidney compared with the control, administration of the oral hypoxia-inducible factor stabilizer enarodustat reversed it, suggesting the pathological improvement. In this way, CUBIC-kidney can provide comprehensive, macroscopic perspective for the kidney research.
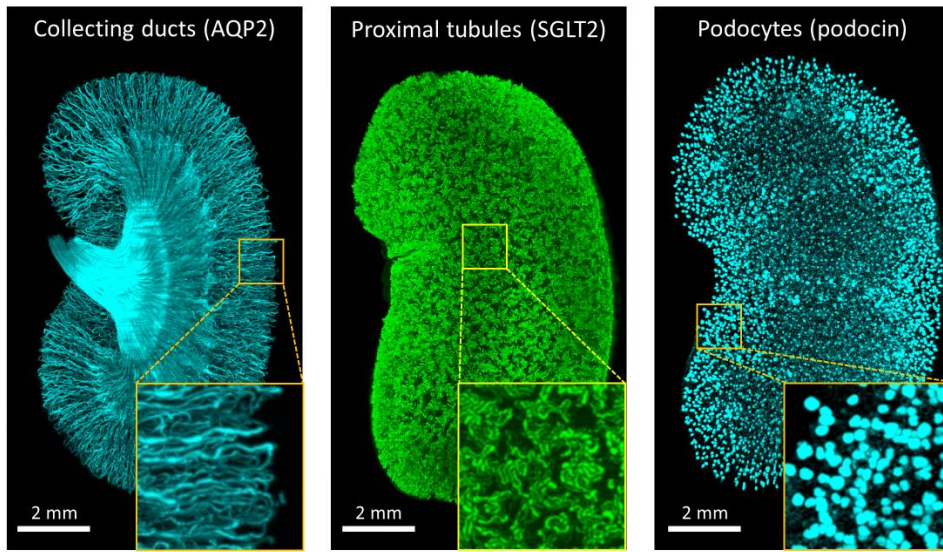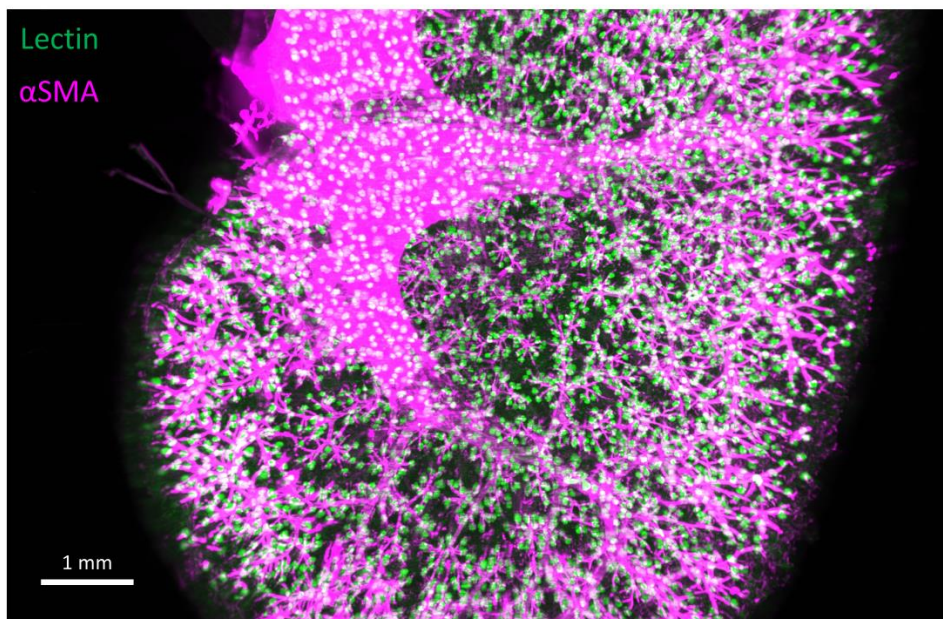
Figure 13. Other applications of CUBIC-kidney

(A) The structure of collecting ducts (AQP2; left), early proximal tubules (SGLT2; middle) and glomeruli (podocin; right). (B) The spatial distribution of glomeruli and arteries visualized by combining fluorescent labeled-lectin perfusion and 3D immunofluorescent staining with αSMA. Glomeruli, in which capillaries are highly accumulated, are particularly recognized after lectin perfusion in a macroscopic viewpoint, although lectin perfusion labels all the vascular endothelial cells. Glomeruli are botryoidally distributed around arteries. AQP2; aquaporin 2, SGLT2; sodium-glucose cotransporter 2, αSMA; alpha smooth muscle actin.
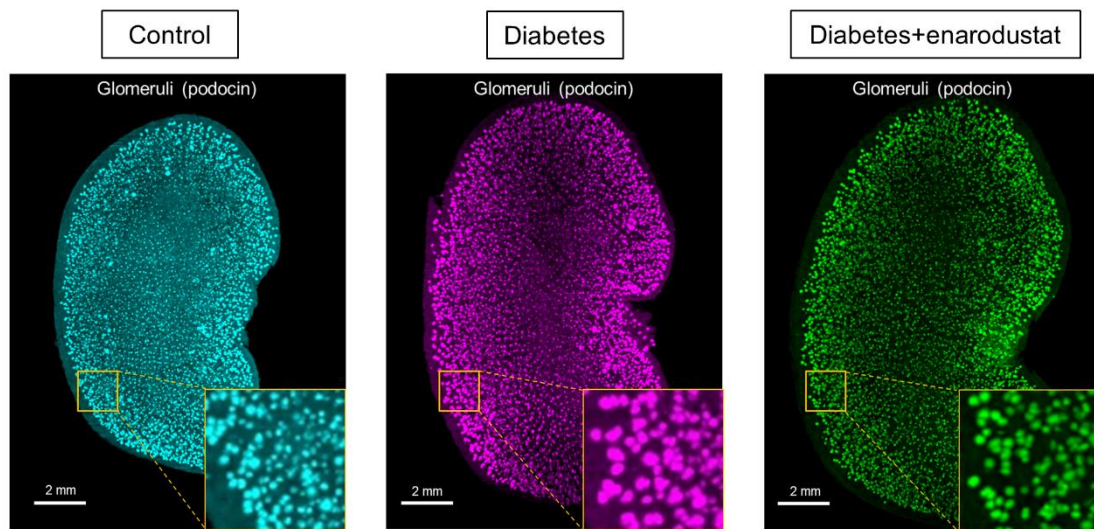
Figure 14. Analysis of glomerular volume using CUBIC-kidney

CUBIC-kidney visualized glomeruli in the whole kidney as shown in Figure 13.
Glomerulomegaly was noticeable in the diabetic kidney compared with the control,
which was reversed by the oral hypoxia-inducible factor stabilizer enarodustat.

Discussion

In this study, I simultaneously visualized the 3D structure of sympathetic

nerves and arteries in kidney tissue, using the combination of tissue clearing methods

(CUBIC), 3D double-immunofluorescent staining, and high-throughput observation by

LSFM. My results have shown that renal sympathetic nerves are primarily distributed

around arteries in the kidney, which is compatible with previous reports that

sympathetic innervation plays an important role in the functional control of blood

vessels in various organs [15]. Moreover, I visualized the 3D structure of collecting

ducts (AQP2), early segments of proximal tubules (SGLT2) and glomeruli (podocin or

lectin perfusion) of mouse kidneys by using 3D immunofluorescent staining. Given the

fact that my group has already succeeded in the identification and segmentation of

glomeruli after nuclear staining of a human kidney block [6], there is a possibility that

3D immunofluorescent staining is also compatible with human kidney samples and can

be applied to clinical renal pathology in the future.

I also characterized a method for quantification of 3D immunofluorescent data

from kidney tissue. Quantification of 3D imaging data demonstrated that the expression

of TH, which is the rate-limiting enzyme of catecholamine synthesis in sympathetic

nerves, was significantly reduced in injured kidneys, suggesting functional abnormality

33

of sympathetic nerves. Moreover, NE levels in kidney tissue were significantly reduced in injured kidneys compared with healthy kidneys, which confirmed the sympathetic denervation after IRI. Sympathetic nerves are important in maintaining the homeostasis of renal functions; this is the first study to clearly visualize sympathetic nervous abnormality after IRI, providing an example of the application of CUBIC methods to kidney research.

However, there remains a lack of clarity regarding the pathophysiological significance of sympathetic denervation after IRI. In the field of cardiology, catecholamine levels in heart tissue have been reported as paradoxically depleted in the failing heart, despite elevated central sympathetic nervous activity [16]. This paradox arises from reduced catecholamine reuptake [17] and reduced catecholamine synthesis [18], in association with the reduction in TH-positive nerves in hearts that have experienced chronic heart failure [15, 19, 20]. My present study has suggested that the same event occurs during the progression of CKD, for the sympathetic denervation (reduction in TH-positive nerves and NE levels in kidney tissue) is persistent even 28 days after IRI. Then, an interesting question is whether sympathetic denervation after injury observed in heart and kidney is protective for organs or not. Previous studies have reported that sympathetic nerves are activated during the progression of CKD [21,

22]. Considering that artificial renal denervation plays a protective role against CKD progression in animal models [23, 24], sympathetic signaling might deteriorate the pathophysiology of CKD. Thus, there is a possibility that the denervation observed after injury is an adaptive response for maintaining the homeostasis, which also have protective roles against CKD progression. Further studies are needed to understand the precise pathophysiological roles of renal sympathetic denervation observed after injury for the CKD progression.

The renal sympathetic denervation after injury might affect the whole body as well as the kidney itself. Recent studies have shown that interventions in the nervous system such as vagus nerve stimulation [25] and C1 neuron activation [26] might be protective against inflammation through immune systems. Moreover, sympathetic nervous system was reported to play important roles in organ crosstalk such heart-brain-kidney network [27]. Thus, it is another interesting topic whether the renal local denervation after injury affects the whole body including immune systems.

As for the technical aspects, I chose the CUBIC protocol for tissue clearing in my study because it fitted my purpose for the following three reasons. First, CUBIC can accomplish a high degree of transparency, which is compatible with the observation by LSFM as shown in Figure 3. Sca*l*eS cannot attain such a high degree of transparency,

while it can preserve the fine structures of organs after tissue clearing on the electron

microscopic level [8]. Second, CUBIC can prevent fluorescent proteins from quenching

during the process of tissue clearing, which is essential because I am planning to

observe genetically encoded fluorescent proteins in addition to 3D immunofluorescent

staining as the next step. Although iDISCO enables a high degree of transparency like

CUBIC, fluorescent proteins quench after tissue clearing [10]. Moreover, the reagents of

iDISCO are composed of organic solvents and should be used in the fume hood. In

contrast, CUBIC is based on hydrophilic chemicals, which are safer for humans

compared with organic solvents. Third, the CUBIC protocol is simple and reproducible.

The protocol of CLARITY is more complicated than CUBIC and the specialized

electrophoresis chamber is needed to maximize the potential abilities of CLARITY [11].

CUBIC can be a strong tool for comprehensive 3D analysis of the kidney, as

shown in my study; however, many problems remain to be addressed before universal

use in kidney research. First, 3D immunofluorescent staining is technically difficult and

time-consuming. Various factors, such as particle radius of antibodies, concentration of

stains, penetration time, or interactions between stains and sample, are involved in 3D

immunohistochemical cell labeling [1]; thus, it is difficult to determine the best working

conditions for each antibody. The development of a more sophisticated 3D staining

protocol may accelerate the application of 3D analysis by CUBIC within the field of nephrology. Second, site-specific analysis of 3D immunofluorescent data remains unavailable. Although αSMA is expressed in both arterial smooth muscle cells and profibrotic myofibroblasts after IRI [28], my study did not show a significant elevation in the ratio of αSMA-positive volume to total kidney volume in IRI-operated kidneys; this is likely because there are fewer myofibroblasts than arterial smooth muscle cells at this stage in a macroscopic view, and because the site of myofibroblasts is localized to a specific area, such as inner cortex and outer medulla [29]. In the field of neuroscience, image registration methods have been developed for functional magnetic resonance imaging to compare the functional activity of different brains by using the spatial alignment of different samples; this concept was applied to the analysis of transparent mouse brains by CUBIC [2, 30]. If such image registration methods can be established to compare transparent kidney samples, it might be possible to recognize site-specific changes in kidney tissue upon 3D analysis with CUBIC.

In conclusion, CUBIC-kidney clearly visualized the 3D structure of renal sympathetic nerves and showed sympathetic denervation after IRI. This newly developed imaging technique can provide comprehensive, macroscopic perspective for kidney research.

Disclosure

Acknowledgements

References

[1] Susaki EA, Ueda HR. Whole-body and Whole-Organ Clearing and Imaging Techniques with Single-Cell Resolution: Toward Organism-Level Systems Biology in Mammals. *Cell Chem Biol* **23**,137-157,2016.

[2] Susaki EA, Tainaka K, Perrin D, Kishino F, Tawara T, Watanabe TM, Yokoyama C, Onoe H, Eguchi M, Yamaguchi S, Abe T, Kiyonari H, Shimizu Y, Miyawaki A, Yokota H, Ueda HR. Whole-brain imaging with single-cell resolution using chemical cocktails and computational analysis. *Cell* **157**,726-739,2014.

[3] Tainaka K, Kubota SI, Suyama TQ, Susaki EA, Perrin D, Ukai-Tadenuma M, Ukai H, Ueda HR. Whole-body imaging with single-cell resolution by tissue decolorization. *Cell* **159**,911-924,2014.

[4] Susaki EA, Tainaka K, Perrin D, Yukinaga H, Kuno A, Ueda HR. Advanced CUBIC protocols for whole-brain and whole-body clearing and imaging. *Nat Protoc* **10**,1709-1727,2015.

[5] Kubota SI, Takahashi K, Nishida J, Morishita Y, Ehata S, Tainaka K, Miyazono K, Ueda HR. Whole-Body Profiling of Cancer Metastasis with Single-Cell Resolution. *Cell Rep* **20**,236-250,2017.

[6] Tainaka K, Murakami TC, Susaki EA, Shimizu C, Saito R, Takahashi K, Hayashi-

Takagi A, Sekiya H, Arima Y, Nojima S, Ikemura M, Ushiku T, Shimizu Y, Murakami M, Tanaka KF, Iino M, Kasai H, Sasaoka T, Kobayashi K, Miyazono K, Morii E, Isa T, Fukayama M, Kakita A, Ueda HR. Chemical Landscape for Tissue Clearing Based on Hydrophilic Reagents. *Cell Rep* **24**,2196-2210 e2199,2018.

[7] Hama H, Kurokawa H, Kawano H, Ando R, Shimogori T, Noda H, Fukami K, Sakaue-Sawano A, Miyawaki A. Scale: a chemical approach for fluorescence imaging and reconstruction of transparent mouse brain. *Nat Neurosci* **14**,1481-1488,2011.

[8] Hama H, Hioki H, Namiki K, Hoshida T, Kurokawa H, Ishidate F, Kaneko T, Akagi T, Saito T, Saido T, Miyawaki A. ScaleS: an optical clearing palette for biological imaging. *Nat Neurosci* **18**,1518-1529,2015.

[9] Erturk A, Becker K, Jahrling N, Mauch CP, Hojer CD, Egen JG, Hellal F, Bradke F, Sheng M, Dodt HU. Three-dimensional imaging of solvent-cleared organs using 3DISCO. *Nat Protoc* **7**,1983-1995,2012.

[10] Renier N, Wu Z, Simon DJ, Yang J, Ariel P, Tessier-Lavigne M. iDISCO: a simple, rapid method to immunolabel large tissue samples for volume imaging. *Cell* **159**,896-910,2014.

[11] Chung K, Wallace J, Kim SY, Kalyanasundaram S, Andalman AS, Davidson TJ, Mirzabekov JJ, Zalocusky KA, Mattis J, Denisin AK, Pak S, Bernstein H,

Ramakrishnan C, Grosenick L, Gradinaru V, Deisseroth K. Structural and molecular interrogation of intact biological systems. *Nature* **497**,332-337,2013.

[12] Tomer R, Ye L, Hsueh B, Deisseroth K. Advanced CLARITY for rapid and high-resolution imaging of intact tissues. *Nat Protoc* **9**,1682-1697,2014.

[13] Keller PJ, Ahrens MB. Visualizing whole-brain activity and development at the single-cell level using light-sheet microscopy. *Neuron* **85**,462-483,2015.

[14] Schindelin J, Arganda-Carreras I, Frise E, Kaynig V, Longair M, Pietzsch T, Preibisch S, Rueden C, Saalfeld S, Schmid B, Tinevez JY, White DJ, Hartenstein V, Eliceiri K, Tomancak P, Cardona A. Fiji: an open-source platform for biological-image analysis. *Nat Methods* **9**,676-682,2012.

[15] Yokoyama T, Lee JK, Miwa K, Opthof T, Tomoyama S, Nakanishi H, Yoshida A, Yasui H, Iida T, Miyagawa S, Okabe S, Sawa Y, Sakata Y, Komuro I. Quantification of sympathetic hyperinnervation and denervation after myocardial infarction by three-dimensional assessment of the cardiac sympathetic network in cleared transparent murine hearts. *PLoS One* **12**,e0182072,2017.

[16] Kanazawa H, Ieda M, Kimura K, Arai T, Kawaguchi-Manabe H, Matsuhashi T, Endo J, Sano M, Kawakami T, Kimura T, Monkawa T, Hayashi M, Iwanami A, Okano H, Okada Y, Ishibashi-Ueda H, Ogawa S, Fukuda K. Heart failure causes cholinergic

transdifferentiation of cardiac sympathetic nerves via gp130-signaling cytokines in rodents. *J Clin Invest* **120**,408-421,2010.

[17] Merlet P, Valette H, Dubois-Rande JL, Moyse D, Duboc D, Dove P, Bourguignon MH, Benvenuti C, Duval AM, Agostini D, et al. Prognostic value of cardiac metaiodobenzylguanidine imaging in patients with heart failure. *J Nucl Med* **33**,471-477,1992.

[18] Kimura K, Ieda M, Kanazawa H, Yagi T, Tsunoda M, Ninomiya S, Kurosawa H, Yoshimi K, Mochizuki H, Yamazaki K, Ogawa S, Fukuda K. Cardiac sympathetic rejuvenation: a link between nerve function and cardiac hypertrophy. *Circ Res* **100**,1755-1764,2007.

[19] Himura Y, Felten SY, Kashiki M, Lewandowski TJ, Delehanty JM, Liang CS. Cardiac noradrenergic nerve terminal abnormalities in dogs with experimental congestive heart failure. *Circulation* **88**,1299-1309,1993.

[20] Qin F, Vulapalli RS, Stevens SY, Liang CS. Loss of cardiac sympathetic neurotransmitters in heart failure and NE infusion is associated with reduced NGF. *Am J Physiol Heart Circ Physiol* **282**,H363-371,2002.

[21] Blankestijn PJ. Sympathetic hyperactivity in chronic kidney disease. *Nephrol Dial Transplant* **19**,1354-1357,2004.

[22] Neumann J, Ligtenberg G, Klein, II, Koomans HA, Blankestijn PJ. Sympathetic hyperactivity in chronic kidney disease: pathogenesis, clinical relevance, and treatment. *Kidney Int* **65**,1568-1576,2004.

[23] Nagasu H, Satoh M, Kuwabara A, Yorimitsu D, Sakuta T, Tomita N, Kashihara N. Renal denervation reduces glomerular injury by suppressing NAD(P)H oxidase activity in Dahl salt-sensitive rats. *Nephrol Dial Transplant* **25**,2889-2898,2010.

[24] Rafiq K, Noma T, Fujisawa Y, Ishihara Y, Arai Y, Nabi AH, Suzuki F, Nagai Y, Nakano D, Hitomi H, Kitada K, Urushihara M, Kobori H, Kohno M, Nishiyama A. Renal sympathetic denervation suppresses de novo podocyte injury and albuminuria in rats with aortic regurgitation. *Circulation* **125**,1402-1413,2012.

[25] Inoue T, Abe C, Sung SS, Moscalu S, Jankowski J, Huang L, Ye H, Rosin DL, Guyenet PG, Okusa MD. Vagus nerve stimulation mediates protection from kidney ischemia-reperfusion injury through alpha7nAChR+ splenocytes. *J Clin Invest* **126**,1939-1952,2016.

[26] Abe C, Inoue T, Inglis MA, Viar KE, Huang L, Ye H, Rosin DL, Stornetta RL, Okusa MD, Guyenet PG. C1 neurons mediate a stress-induced anti-inflammatory reflex in mice. *Nat Neurosci* **20**,700-707,2017.

[27] Fujiu K, Shibata M, Nakayama Y, Ogata F, Matsumoto S, Noshita K, Iwami S,

Nakae S, Komuro I, Nagai R, Manabe I. A heart-brain-kidney network controls adaptation to cardiac stress through tissue macrophage activation. *Nat Med* **23**,611-622,2017.

[28] Mack M, Yanagita M. Origin of myofibroblasts and cellular events triggering fibrosis. *Kidney Int* **87**,297-307,2015.

[29] Venkatachalam MA, Weinberg JM, Kriz W, Bidani AK. Failed Tubule Recovery, AKI-CKD Transition, and Kidney Disease Progression. *J Am Soc Nephrol* **26**,1765-1776,2015.

[30] Murakami TC, Mano T, Saikawa S, Horiguchi SA, Shigeta D, Baba K, Sekiya H, Shimizu Y, Tanaka KF, Kiyonari H, Iino M, Mochizuki H, Tainaka K, Ueda HR. A three-dimensional single-cell-resolution whole-brain atlas using CUBIC-X expansion microscopy and tissue clearing. *Nat Neurosci* **21**,625-637,2018.